ADVANCED FUNCTIONAL MATERIALS
www.afm-journal.de

Colloid-Mediated Fabrication of a 3D Pollen Sponge for Oil Remediation Applications

Youngkyu Hwang, Mohammed Shahrudin Bin Ibrahim, Jingyu Deng, Joshua A. Jackman, and Nam-Joon Cho**

There is tremendous interest in developing 3D scaffolds from natural materials for a wide range of healthcare, energy, photonic, and environmental science applications. To date, most natural materials that are used to make 3D scaffolds consist of fibril structures; however, it would be advantageous to explore the development of scaffolds from natural materials with distinct supramolecular structures. Herein, the fabrication of a mechanically responsive pollen sponge that exhibits tunable 3D scaffold properties and is useful for oil remediation applications is reported. By using pollen-based microgel particles as colloidal building blocks, the sponge fabrication process is optimized by tuning the processing conditions during freeze-drying and thermal annealing steps. Stearic acid functionalization transforms the pollen sponge into a hydrophobic scaffold that can readily and repeatedly absorb oil and other organic solvents from contaminated water sources, with similar performance levels to commercial, synthetic polymer-based absorbents and an improved environmental footprint.

1. Introduction

3D microporous scaffolds are highly versatile materials that can be used in a wide range of healthcare, energy, photonic, and environmental science applications.[1–5] Most design progress in the field has focused on using synthetic polymers such as polyurethane (PU), polydimethylsiloxane (PDMS), and poly(3,4-ethylenedioxythiophene) (PEDOT).[6–9] Rationally tuning the chemical composition and other molecular features of synthetic polymers enables scaffolds to have advantageous properties, including low density, high surface area, high absorption capacity, and excellent mechanical properties.[10–14] The functionality of polymer-based scaffolds can be further enhanced by incorporating inorganic components such as 1D and 2D nanomaterials, e.g., carbon nanotubes and graphene, that can modulate various scaffold properties, including conductivity, porosity, and compressibility.[15–17]

At the same time, there is growing concern about the environmental impact of synthetic polymer-based scaffolds and a desire to instead use natural materials such as cellulose, collagen, and silk that are affordable, plentiful, renewable, and biodegradable.[18–21] Attention to this topic falls in line with current trends to view renewable biomass as a promising source for developing advanced materials.[22–24] To date, most natural materials that are used to make 3D scaffolds consist of fibril structures while it would be advantageous to explore the development of scaffolds from natural materials that self-assemble into other types of supramolecular structures. One excellent candidate is natural pollen grains, which are renewably produced in abundant supply by plants and possess many attractive material properties, including hollow microcapsule structure, chemical stability, mechanical strength, species-specific architectural details, and high monodispersity among each species of pollen grains.[25–30]

For a long time, the basic structural properties of pollen grains were regarded as unchangeable, in large part owing to the presence of sporopollenin—considered the "diamond of biopolymers"—in the outer layer of the pollen shell called the exine.[31] As such, most investigations focused on exploring discrete pollen grains as markers for environmental dating (palynology) as well as drug delivery carriers.[32–34] More recently, it was reported that hard pollen grains are in fact pliable and can be converted into soft, stimuli-responsive microgel particles based on a simple chemical process akin to soapmaking, which adjusts the mechanical properties of the pollen shell layers.[35] This discovery has opened the door to developing self-actuating paper sheets derived from self-assembling microgel particles and further motivates the exploration of advanced material fabrication strategies to create 3D scaffolds composed exclusively of pollen grains.[36] It is also advantageous that pollen grains—both in the natural form and as isolated exine capsules—possess a myriad of useful functional groups, including extensive

Dr. Y. Hwang, M. S. B. Ibrahim, J. Deng, Prof. N.-J. Cho
School of Materials Science and Engineering
Nanyang Technological University
50 Nanyang Avenue, Singapore 639798, Singapore
E-mail: njcho@ntu.edu.sg
Dr. Y. Hwang, Prof. J. A. Jackman
School of Chemical Engineering
Sungkyunkwan University
Suwon 16419, Republic of Korea
E-mail: jjackman@skku.edu
Dr. Y. Hwang, Prof. J. A. Jackman
Biomedical Institute for Convergence at SKKU (BICS)
Sungkyunkwan University
Suwon 16419, Republic of Korea
The ORCID identification number(s) for the author(s) of this article can be found under https://doi.org/10.1002/adfm.202101091.

DOI: 10.1002/adfm.202101091

surface hydroxylation, that can facilitate covalent and noncovalent attachment depending on the application.[31,37]

Herein, we report the fabrication of a mechanically responsive pollen sponge that exhibits tunable 3D scaffold properties and is useful for oil remediation applications. By using pollen-based microgel particles as colloidal building blocks, the sponge fabrication process was optimized by tuning the processing conditions during freeze-drying and thermal annealing steps. Subsequently, the simple attachment of stearic acid—one of the most common fatty acid molecules in nature—transformed the pollen sponge into a hydrophobic scaffold that could readily and repeatedly absorb oil and other organic solvents from contaminated water sources, with similar performance levels to commercial, synthetic polymer-based absorbents and an improved environmental footprint.

2. Results and Discussion

Figure 1 presents an overview of the pollen sponge fabrication process, starting with the sourcing of natural pollen grains from sunflower plants (*Helianthus annuus*) that had been collected by bees. The natural pollen grains of ≈20-µm diameter are hollow microcapsules with a two-layer wall structure that is perforated by apertures, and the entire grain surface is covered with lipidic components commonly referred to as pollen cement (Figure 1a and Figure S1, Supporting Information). To first remove this lipidic cement ("defatting"), we sequentially rinsed the pollen grains with water, acetone, and diethyl ether (Figure 1b). The pollen grains were then refluxed in an aqueous potassium hydroxide solution (KOH, 10 wt/vol%) at 80 °C for 2 h to remove inner contents, resulting in the pollen shell only (Figure 1c).

The resulting pollen shells were further incubated in fresh KOH solution for varying time durations between 0 and 72 h, before freeze-drying them at −20, −80, or −196 °C for 2 d to induce pollen wall lamination owing to ice crystal nucleation (Figure 1d–f).[38,39] These processes resulted in the formation of pollen sponges with 3D porous architectures and inclusion of the second KOH incubation step led to decreases in both material density and mechanical strength (Figure S2, Supporting Information). Scanning electron microscopy (SEM) imaging further verified that, during this second step, longer incubation times up to 72 h improved sponge fabrication quality, as indicated by a progressively lower number of defects in the sponge walls (Figure S3, Supporting Information). The freezing temperature was also an important parameter and more homogenous sponge structures were obtained at −20 °C, as indicated by relatively smooth, partially delaminated walls that are advantageous for high levels of surface attachment (Figure S4, Supporting Information). These morphological features stand out in comparison to the typically observed, highly porous walls of 3D sponge scaffolds formed from fibril-like natural materials,[40,41] and the use of highly uniform pollen grains in this fabrication strategy provides a similar templating function to colloidal microparticles used in designing inverted colloidal crystal scaffolds, for example.[42]

The as-obtained pollen sponges were then briefly heated at 150, 200, 250, or 300 °C for 10 min and sponge structures heated at 200 °C or higher temperatures remained morphologically stable after aqueous hydration and subsequent dehydration (Figure S5, Supporting Information). We selected 200 °C as the temperature for heating, and the Young's modulus value of the sponge structure upon heating also increased by over twofold as compared to the sponge structure without heating, while the volume change was small (Figure S6, Supporting Information). Finally, the sponge structure was incubated in an ethanolic solution containing stearic acid—one of the most common fatty acids found in nature—for 1 h and the stearic acid molecules noncovalently attached to the sponge walls to render them highly hydrophobic while maintaining structural integrity.

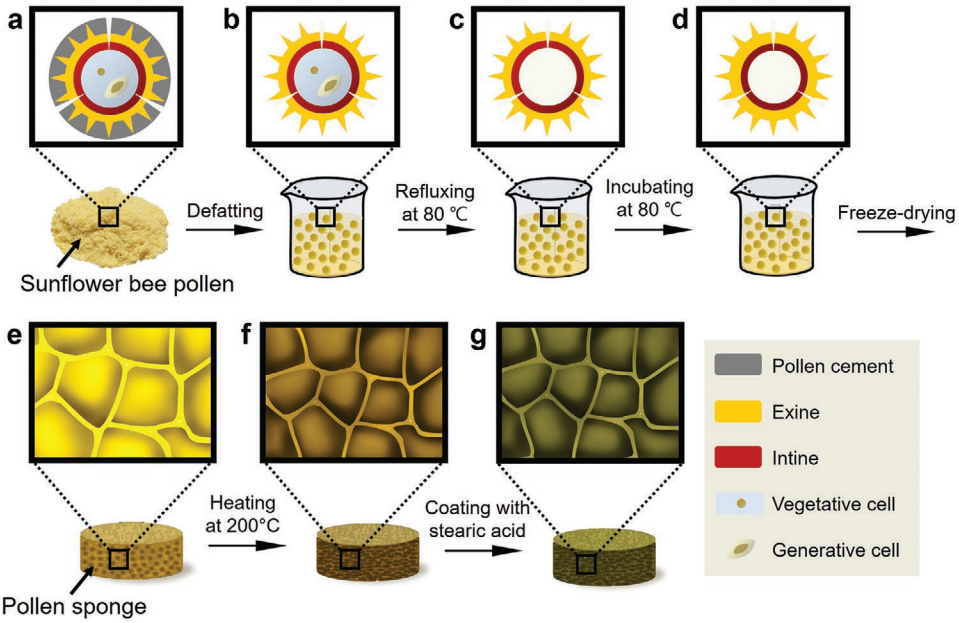

Figure 1. a–g) Schematic illustration of the step-by-step fabrication process to prepare oil-absorbing pollen sponges.

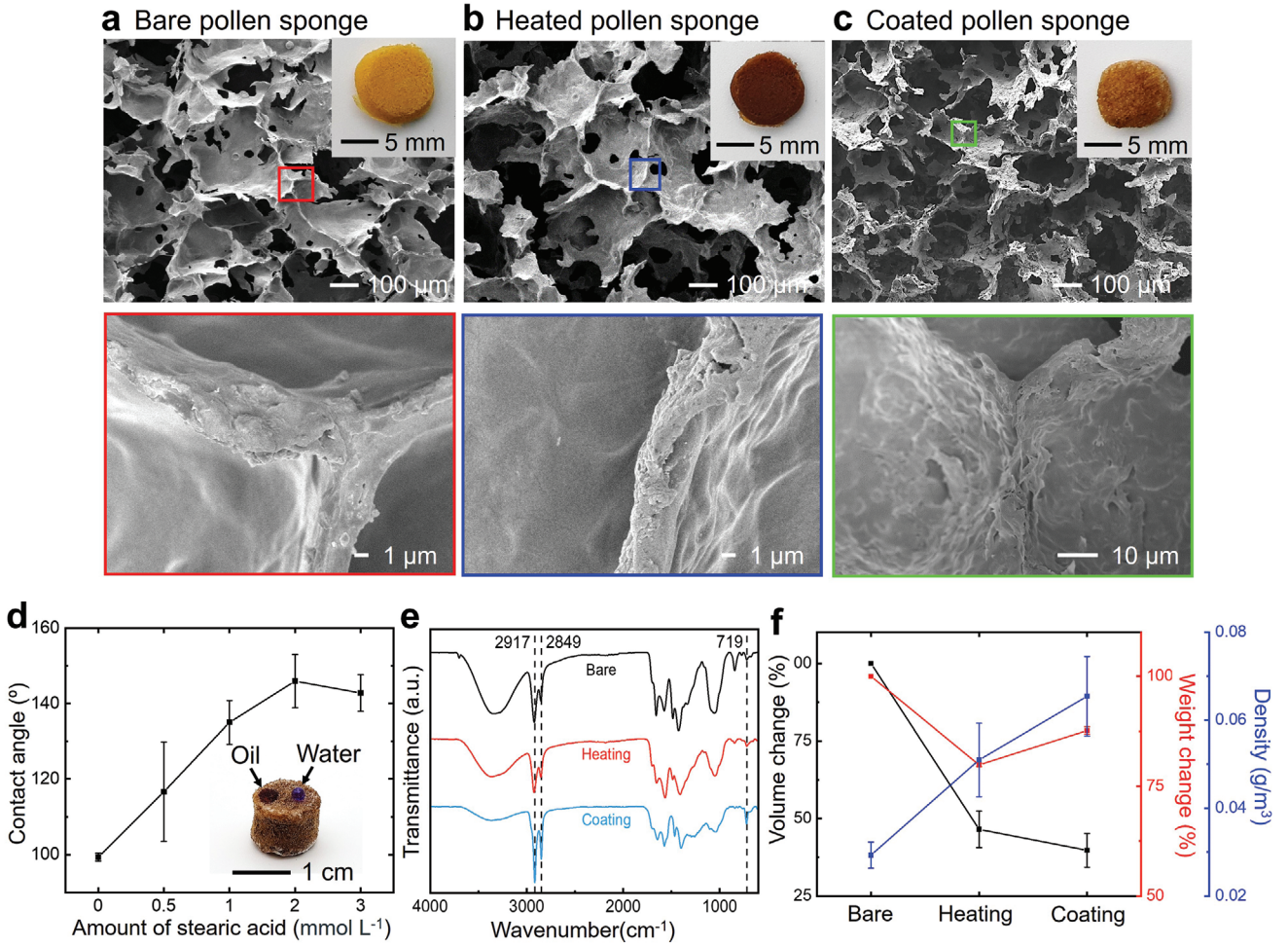

Figure 2. Structural characterization of pollen sponges. a–c) Cross-sectional SEM images of bare, heated, and coated pollen sponges. The red, blue, and green boxes correspond to magnified images of the selected areas in each image. d) Water contact angle of the pollen sponge after coating with different concentrations of stearic acid. e) FTIR spectroscopic analysis of bare, heated, and coated pollen sponges. f) Volume, weight, and density of pollen sponges at different fabrication stages.

The fabricated pollen sponges were characterized by SEM imaging before and after heating and after stearic acid functionalization. The bare sponge had a light brown color and highly porous structure owing to lamination of the pollen walls (**Figure 2**a and Figure S7, Supporting Information). Upon heating, the sponge structure assumed a dark brown color while retaining microstructural features of the bare sponge (Figure 2b). After stearic acid coating, the sponge structure had a brown color and maintained the 3D porous architecture along with apparently decreased pore area owing to ethanol-induced shrinkage (Figure 2c).

We further investigated how the bulk stearic acid concentration used to coat heat-treated sponges affected resulting sponge hydrophobicity. Concentration-dependent increases in sponge hydrophobicity were observed for up to 2×10^{-3} M stearic acid concentrations, which signifies that the maximum binding capacity of the sponge was reached and resulted in a maximum water contact angle (WCA) of 145° (Figure 2d). At higher concentrations, the hydrophobicity tended to slightly decrease, which may result from stearic acid forming a double layer on the sponge wall surface that would expose hydrophilic carboxylic acid groups.[43,44] Hence, we selected 2×10^{-3} M stearic acid as the optimal coating condition. Fourier-transform infrared (FTIR) spectroscopy experiments were also performed to characterize structural changes related to heat treatment and stearic acid coating (Figure 2e). It was observed that three peaks (2917, 2849, and 719 cm^{-1}), which are related to C—H bonds, decreased after heating owing to protein and lipid degradation, while the peaks increased again upon stearic acid coating.[45–47] In line with these results, cross-sectional SEM images supported that the coated sponges had smaller pore areas than the other sponges (**Table 1**). The coated sponges had a final density

Table 1. Density and pore area of pollen sponges.

Sample	Density [g cm^{-3}]	Pore area [μm^2]
Bare	$2.9 \times 10^{-5} \pm 3.0 \times 10^{-6}$	$7.3 \times 10^4 \pm 1.2 \times 10^4$
Heated	$5.1 \times 10^{-5} \pm 8.4 \times 10^{-6}$	$5.7 \times 10^4 \pm 1.3 \times 10^4$
Coated	$6.5 \times 10^{-5} \pm 9.1 \times 10^{-6}$	$3.4 \times 10^4 \pm 8.2 \times 10^3$

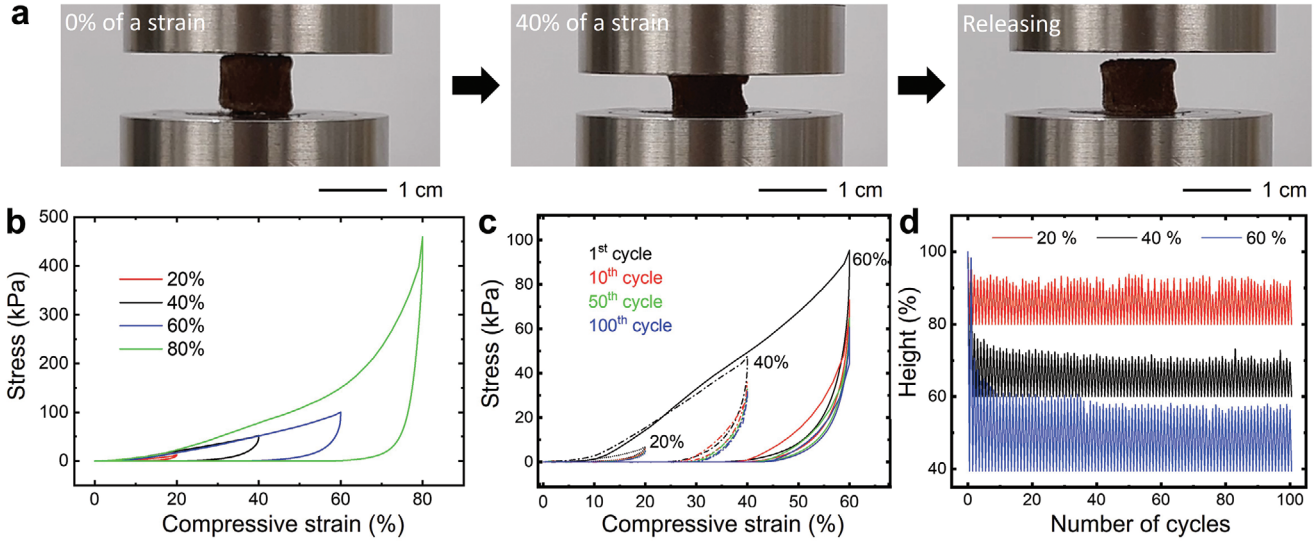

Figure 3. Mechanical characterization of pollen sponges. a) Photographs of reversible compression of pollen sponge under 40% compressive strain. b) Strain–stress curves of pollen sponge under 20%, 40%, 60%, and 80% compressive strains. c) Strain–stress curves of pollen sponges with cyclic compression under 20%, 40%, and 60% compressive strains. d) Change in height profile of pollen sponges during 100 cycles of compression under 20%, 40%, and 60% compressive strains.

around 0.065 cm^{-3}, which is comparable to the densities of sponges fabricated from bacterial cellulose, graphene, and carbon nanotubes (Figure 2f).[48]

Another important property of oil-absorbing materials is compressibility, whereby oil-laden sponges can be compressed to release the oil waste and then reused. Mechanical tests were conducted on the coated sponges with varying degrees of compressive strain (20%, 40%, 60%, and 80%, respectively). **Figure 3**a shows sequential photographs of a pollen sponge with no strain, 40% compressive strain, and in the recovered state upon release. The pollen sponge retained ≈90% of its original height after release. We also measured stress–strain curve at compressive strains of 20%, 40%, 60%, and 80%. The hysteresis loops of the samples under compressive strains of 20%, 40%, and 60% had a cyclical shape indicative of elastic deformation (Figure 3b). However, with 80% compressive strain, there was a sharp increase in stress that was caused by structural collapse and

Figure 4. Oil absorption capacity of pollen sponge. a,b) Photographs of sponge-mediated removal of silicone oil and dichloromethane from contaminated water samples, respectively. Silicone oil and dichloromethane were premixed with lipophilic red dye for high optical contrast.

densification of the sponge structure (Figure S8, Supporting Information).

Cyclical compression tests at 20%, 40%, and 60% compressive strains were also conducted, and minor changes in the stress–strain curves were observed after the tenth cycle (Figure 3c). Similar curve profiles were observed at the 50th and 100th cycles. The change in height of the pollen sponge samples was also measured during the cyclical compression testing (Figure 3d). After the first compression cycle, the pollen sponges recovered ≈98% of their original height for up to 80% compressive strain (Figure S9, Supporting Information). With subsequent compression cycles, the pollen sponges became conditioned and maintained structural integrity with tempered but consistent height recovery trends. After 100 cycles, the pollen sponges retained ≈92%, 72%, and 59% of their original height upon 20%, 40%, and 60% compressive strains, respectively. Together, these data support that elastic deformation and partial structural collapse ("conditioning") of the pollen sponge occurred during the first few compression cycles and structural stabilization was achieved after five to ten cycles.

To characterize the functional performance of the coated pollen sponge, we performed oil absorption tests with various oils and organic solvents. **Figure 4**a,b shows the performance of pollen sponges to remove silicone oil (density of 0.971 g mL^{-1}) and dichloromethane (density of 1.33 g mL^{-1}) from the surface and bottom of water samples, respectively (Videos S1 and S2, Supporting Information). The oils were labeled with a red, lipophilic dye for visualization and complete absorption of the oils was achieved in both cases without water absorption. In the latter case of dichloromethane absorption, an air bubble was observed during the extraction process, which indicated mass exchanged between air and dichloromethane within the sponge structure.

We also tested the oil absorption capability of the pollen sponge to sequester various types of oils and organic solvents with different densities (**Figure 5**a). In general, the pollen sponge exhibited greater than 10 g g^{-1} absorption capacity and the maximum absorption capacity was over 29.3 g g^{-1} for chloroform, while the minimum was 9.7 g g^{-1} for coconut oil. This performance range is comparable to commercial polypropylene absorbents (8.1–24.6 g g^{-1}).[49] We also further characterized the reusability of the pollen sponge for oil absorption applications in cyclical performance tests (Figure 5b). We repeated ten cycles of soaking the pollen sponge in silicone oil for 5 min,

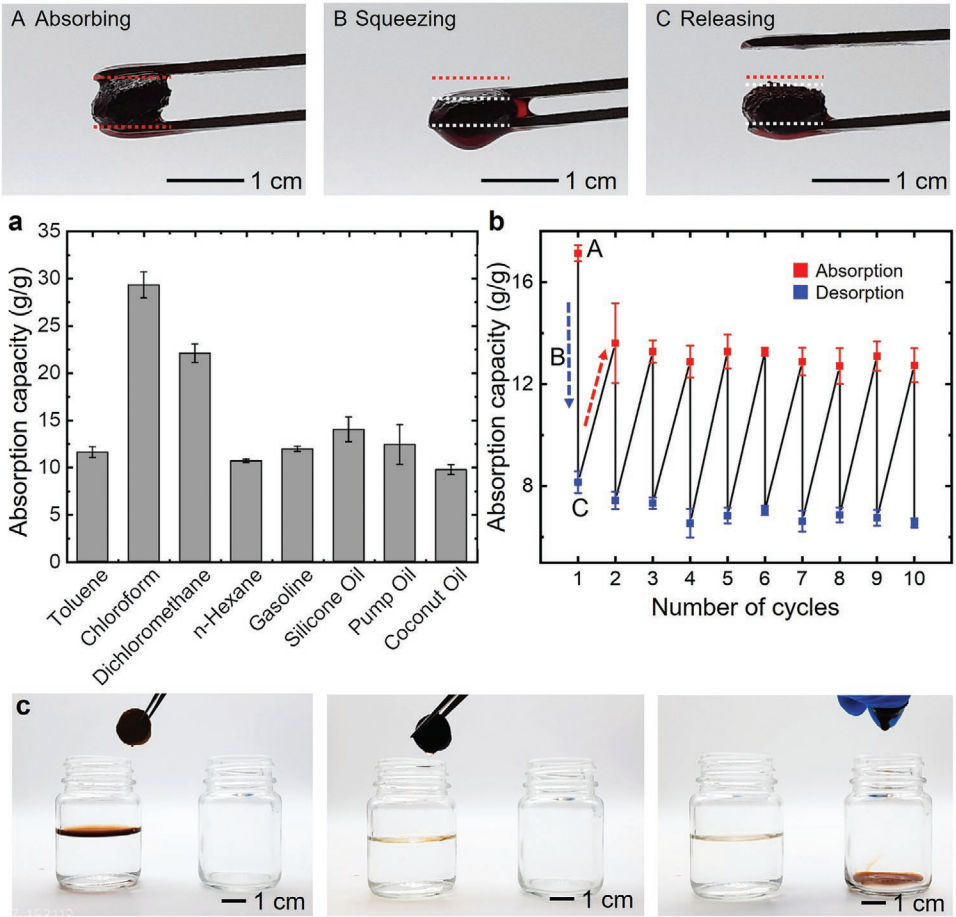

Figure 5. Performance testing and reusability of oil-absorbing pollen sponge. a) Mass-based absorption capacity of pollen sponge for various oils and organic solvents. b) Cyclical testing of pollen sponge absorption capacity for silicone oil. The absorption and release amounts are reported for each cycle. Photographs in top row correspond to the absorbing (A), squeezing (B), and releasing (C) steps. c) Absorption, removal, and squeeze-mediated release of motor oil from contaminated water sample by using a pollen sponge.

squeezing the sponge until reaching ≈45% compression, and then repeating the process. During the first cycle, the pollen sponge absorbed 17.1 g g^{-1} of oil, and 9.0 g g^{-1} of oil was released by squeezing. In subsequent cycles, the pollen sponge consistently achieved 13.6 g g^{-1} absorption and 6.2 g g^{-1} release for up to 10 cycles, supporting that the pollen sponges are durable and reusable.

In one final proof-of-concept experiment, we investigated the ability of a pollen sponge to remove motor oil from a contaminated water sample (Figure 5c). The sponge readily absorbed the motor oil in less than 2 min, and then the motor oil was released into a separate container through the squeezing method (Video S3, Supporting Information). Collectively, these results demonstrate that the pollen sponge can selectively absorb and release oil contaminants and has similar performance levels to commercial oil absorbents while demonstrating compelling properties such as low cost, biocompatibility, and sustainable production. The hydrophobic surface character of the pollen sponge in this case was facilitated by noncovalent attachment of stearic acid molecules while there is broad potential to also develop hydrophilic versions of the pollen sponge scaffold by incorporating processing strategies such as ultraviolet–ozone treatment.[50]

3. Conclusion

In this study, we developed an oil-absorbing pollen sponge that is derived from low-cost bee pollen microcapsules. While pollen grains not used for plant pollination are often considered biological waste, we demonstrate that they can be readily fabricated into 3D sponge architectures using a colloid-based strategy and coating the sponge with a naturally abundant fatty acid can transform the sponge into an oil-absorbing material. Importantly, all of the fabrication steps are straightforward and environmentally friendly. While other types of natural materials, typically composed of fibril structures, have been used to fabricate 3D scaffolds in past works, our findings demonstrate the potential of using spongy pollen particles—engineered from natural pollen grains to exhibit microgel-like behavior—as the colloidal building blocks to fabricate mechanically responsive sponges. Such findings expand the range of natural materials that can be used to fabricate 3D scaffolds and open the door to new classes of porous, advanced materials derived from pollen particles.

4. Experimental Section

Defatting of Sunflower Bee Pollen Granules: Sunflower bee pollen granules were purchased from GTL Biotech (Xi'an, Shaanxi, China) and defatted by first dispersing 250 g of the sample in deionized water (1000 mL) and stirring. The suspension was filtered through nylon mesh with 200 µm pore size (ELKO Filtering Co., USA). The dispersed pollen in the filtrate was collected via vacuum filtration using a Büchner funnel lined with filter paper. The collected pollen was refluxed in 500 mL acetone (Aik Moh, Singapore) at 50 °C for 3 h under continuous stirring. The acetone in the suspension was removed by vacuum filtration as before and the collected pollen was washed with fresh acetone followed by vacuum filtration. This washing step was repeated five times. The acetone reflux and washing processes were repeated again. The resulting pollen powder was transferred into a glass petri dish and air-dried overnight in a fume hood.

The dried pollen powder (≈120 g) was suspended in 200 mL diethyl ether (Sigma Aldrich, Singapore) and continuously stirred at room temperature for 2 h. The diethyl ether in the suspension was removed by vacuum filtration, and the collected pollen was washed with fresh diethyl ether followed by vacuum filtration. This washing process was repeated three times. The collected pollen was suspended in diethyl ether (200 mL) again and continuously stirred at room temperature overnight, and the washing process was repeated. The resulting pollen powder was transferred to a glass petri dish and air-dried overnight in a fume hood. The dry defatted pollen was collected in a plastic bottle and stored in a desiccator cabinet under low humidity conditions until use.

Sponge Fabrication: Defatted pollen was initially transformed into microgel particles following previous protocols[35] with slight modification. 2 g of defatted sunflower pollen was suspended in 20 mL of 10% w v^{-1} KOH solution in a polytetrafluoroethylene (PTFE) round-bottom flask. The suspension was continuously stirred and refluxed for 2 h at 80 °C. The pollen was isolated via filtration using a nylon mesh with 20 µm pore size, and the collected pollen was rinsed with 20 mL of 10% w v^{-1} KOH followed by filtration. The rinsing and filtration process were repeated a total of three times. The rinsed pollen was transferred to a 50 mL conical centrifuge tube and topped up to a total volume of 20 mL with fresh KOH solution. The solution was resuspended using a vortex mixer at high speed for 2 min and was incubated at 80 °C in an oven (Memmert, Schwabach, Germany) for defined periods of time (6, 12, 24, 48, and 72 h).

After incubation, the pollen particles were isolated via filtration using a nylon mesh with 20 µm pore size. The collected pollen was rinsed with copious amounts of deionized water followed by filtration. The rinsing and filtration processes were repeated until the pH of the suspension reached 7, as measured by using pH-indicator strips (Millipore Sigma, Burlington, MA). The resulting neutral-pH pollen microgel suspension was transferred to a 50 mL conical centrifuge and centrifuged at 3000 rpm (Beckman Coulter, Allegra X-15 R, rotor SX4750) for 5 min. The residual water supernatant was then decanted.

The as-prepared pollen microgel was then pipetted into individual wells of Nunc 24-well tissue culture dishes (Thermo Scientific, Rochester, NY), and the plates were centrifuged at 3000 rpm (Beckman Coulter, Allegra X-15 R, rotor SX4750µ) for 15 min to remove any residual water. The plates were then frozen in the freezers overnight or in liquid nitrogen for 15 min. The plates containing the frozen microgel were lyophilized (Labconco, Kansas City, MO) under 0.008 mbar vacuum for 48 h to obtain the bare pollen sponges. Heat-treated pollen sponges were prepared by incubating the bare pollen sponges in a furnace (XST-3-0-12-1V2, Thermcraft, USA) at the specified temperature for 30 min. Coated pollen sponges were prepared by immersing heat-treated sponges in ethanolic solutions of stearic acid for 60 min and left to dry at room temperature overnight. Individual pollen sponge samples were weighed and geometrical dimensions were measured via Vernier calipers to determine their density. Contact angle measurements were performed using an Attension Theta Optical Tensiometer (Biolin Scientific AB, Sweden) via the sessile drop method. 20 µL of deionized water was dispensed onto the pollen sponge surface, and the shape of the drop was recorded by high-resolution imaging. For analysis, the drop shape was fitted to the Young–Laplace equation, and the duration of each measurement was 10 s.

Mechanical Testing: The compressive Young's modulus values of the pollen sponges were analyzed using a DMA Q800 dynamic mechanical analyzer (TA Instruments, USA) in a controlled force mode. The pollen sponge samples were held between parallel-plate compression clamps and were then compressed at a 1 N min^{-1} ramp rate from 0.1 to 18.0 N. The compressive Young's modulus was calculated from the slope of the elastic region of the stress–strain curve, between 40% and 50% compressive strain. Cyclical compression recovery analyses of the pollen sponges were performed on the MTS Criterion Model 42 instrument (MTS Systems Corporation, USA). Pollen sponges were subjected to

100 cycles of 1 mm min^{-1} compression up to the determined compressive strain and 0.01 mm min^{-1} decompression back to the original sample height.

Morphological Analysis of Pollen Sponges: High-magnification images of pollen sponge cross sections were obtained via field emission-scanning electron microscopy (FESEM). Pollen sponges were gently sliced with a sharp blade along the transverse plane and immobilized on the sample holder with carbon tape and sputter-coated with platinum to a thickness of 5 nm (20 mA, 40 s) using a JFC-1600 Auto Fine Coater (JEOL, Tokyo, Japan) to improve the sample conductivity. Thick samples were further held in place using copper tape. Images were taken with a JSM-7600F Schottky microscope (JEOL) at an acceleration voltage of 5.00 kV. Pollen sponge cross-sectional pore area was determined via measurement of the obtained images via ImageJ (NIH, USA). A minimum of 30 pores showing intact borders was used to calculate the results for each sample.

Fourier-Transform Infrared Spectroscopy: FTIR spectroscopic analysis of the pollen sponge was conducted using the PerkinElmer Spectrometer (PerkinElmer, UK) equipped with a diamond cell attenuated total reflection (ATR) accessory. Reflectance infrared spectra were obtained between 4000 and 600 cm^{-1} by 16-times scanning per measurement. For each sample, three different areas were measured. Background spectra were collected prior to sample readings and subtracted from each sample spectrum automatically by Spectrum 10 Software (PerkinElmer, UK). To correct spectra with sloped baselines and reduce the amount of noise in the spectrum, a baseline correction and smoothing process were conducted after sample measurements using the software.

Oil Absorption Capacity Measurement: Silicone oil (ρ = 0.971 g cm^{-3}, Sigma-Aldrich) and dichloromethane (ρ = 1.33 g cm^{-3}, VWR Chemicals) were mixed with lipophilic Oil Red O dye (molecular weight = 408.49 g mol^{-1}, Sigma-Aldrich) for high optical contrast and then mixed with water samples. A coated pollen sponge after drying in an oven at 60 °C for 2 h was used for the testing. To test oil absorption to various oils and organic solvents, the oil absorption capacity (g g^{-1}) was calculated by the following equation:

$$\text{Absorption capacity}\left(\text{g g}^{-1}\right) = (w - w_0)/w_0 \quad (1)$$

where w_0 is the weight of the coated pollen sponge after drying, and w is the weight of the coated pollen sponge after oil absorption. The pollen sponge was immersed into the various oils and organic solvents [toluene (ρ = 0.865 g cm^{-3}, Sigma-Aldrich), chloroform (ρ = 1.49 g cm^{-3}, Sigma-Aldrich), dichloromethane (ρ = 1.33 g cm^{-3}, VWR Chemicals), *n*-hexane (ρ = 0.659 g cm^{-3}, Sigma-Aldrich), gasoline (Synergy Extra 5000, Esso), silicone oil (ρ = 0.971 g cm^{-3}, Sigma-Aldrich), pump oil (ρ = 0.859 g cm^{-3}, Edwards), motor oil (ρ = 0.861 g cm^{-3}, 7100 10w40, Motul), and coconut oil (Marico)] for 5 min.

Supporting Information

Supporting Information is available from the Wiley Online Library or from the author.

Acknowledgements

Y.H. and M.S.B.I. contributed equally to this work. This research was supported by the MOTIE (Ministry of Trade, Industry, and Energy) in Korea, under the Fostering Global Talents for Innovative Growth Program (P0008746) supervised by the Korea Institute for Advancement of Technology (KIAT). In addition, this work was supported by the SKKU Research Fellowship Program of Sungkyunkwan University.

Conflict of Interest

The authors declare no conflict of interest.

Data Availability Statement

Research data are not shared.

Keywords

3D scaffolds, biological materials, colloids, pollen grains, porous materials

Received: February 1, 2021
Revised: February 16, 2021
Published online:

[1] A. Chhetry, S. Sharma, H. Yoon, S. Ko, J. Y. Park, *Adv. Funct. Mater.* **2020**, *30*, 1910020.
[2] W. Fan, N. W. Li, X. Zhang, S. Zhao, R. Cao, Y. Yin, Y. Xing, J. Wang, Y. G. Guo, C. Li, *Adv. Sci.* **2018**, *5*, 1800559.
[3] M. Wang, N. Zhang, Y. Tang, H. Zhang, C. Ning, L. Tian, W. Li, J. Zhang, Y. Mao, E. Liang, *J. Mater. Chem. A* **2017**, *5*, 12252.
[4] F. Giorgianni, C. Vicario, M. Shalaby, L. D. Tenuzzo, A. Marcelli, T. Zhang, K. Zhao, Y. Chen, C. Hauri, S. Lupi, *Adv. Funct. Mater.* **2018**, *28*, 1702652.
[5] P. Cherukupally, W. Sun, A. P. Y. Wong, D. R. Williams, G. A. Ozin, A. M. Bilton, C. B. Park, *Nat. Sustainability* **2019**, *3*, 136.
[6] S. Zhang, H. Liu, S. Yang, X. Shi, D. Zhang, C. Shan, L. Mi, C. Liu, C. Shen, Z. Guo, *ACS Appl. Mater. Interfaces* **2019**, *11*, 10922.
[7] S. Zhao, R. Zhu, *Adv. Mater. Technol.* **2019**, *4*, 1900414.
[8] T. Zhou, J. Yang, D. Zhu, J. Zheng, S. Handschuh-Wang, X. Zhou, J. Zhang, Y. Liu, Z. Liu, C. He, X. Zhou, *Adv. Sci.* **2017**, *4*, 1700028.
[9] X. Qi, T. Miao, C. Chi, G. Zhang, C. Zhang, Y. Du, M. An, W.-G. Ma, X. Zhang, *Nano Energy* **2020**, *77*, 105096.
[10] Z. Li, K. Hu, M. Yang, Y. Zou, J. Yang, M. Yu, H. Wang, X. Qu, P. Tan, C. Wang, X. Zhou, Z. Li, *Nano Energy* **2019**, *58*, 852.
[11] C. Ruan, K. Ai, X. Li, L. Lu, *Angew. Chem., Int. Ed. Engl.* **2014**, *53*, 5556.
[12] L. Zhu, J. Ji, J. Liu, S. Mine, M. Matsuoka, J. Zhang, M. Xing, *Angew. Chem., Int. Ed. Engl.* **2020**, *59*, 13968.
[13] S. Jiang, J. Y. Cheong, J. S. Nam, I. D. Kim, S. Agarwal, A. Greiner, *ACS Appl. Mater. Interfaces* **2020**, *12*, 19006.
[14] L. Wu, L. Li, B. Li, J. Zhang, A. Wang, *ACS Appl. Mater. Interfaces* **2015**, *7*, 4936.
[15] Y. Song, H. Chen, Z. Su, X. Chen, L. Miao, J. Zhang, X. Cheng, H. Zhang, *Small* **2017**, *13*, 1702091.
[16] F. Zhang, Y. Feng, M. Qin, L. Gao, Z. Li, F. Zhao, Z. Zhang, F. Lv, W. Feng, *Adv. Funct. Mater.* **2019**, *29*, 1901383.
[17] B. Li, S. B. Yang, S. M. Li, B. Wang, J. H. Liu, *Adv. Energy Mater.* **2015**, *5*, 1500289.
[18] Y. Li, L. Xu, B. Xu, Z. Mao, H. Xu, Y. Zhong, L. Zhang, B. Wang, X. Sui, *ACS Appl. Mater. Interfaces* **2017**, *9*, 17155.
[19] G. Wang, Y. He, H. Wang, L. Zhang, Q. Yu, S. Peng, X. Wu, T. Ren, Z. Zeng, Q. Xue, *Green Chem.* **2015**, *17*, 3093.
[20] Y. Wang, D. B. Gunasekara, M. I. Reed, M. DiSalvo, S. J. Bultman, C. E. Sims, S. T. Magness, N. L. Allbritton, *Biomaterials* **2017**, *128*, 44.
[21] L. Tozzi, P. A. Laurent, C. A. Di Buduo, X. Mu, A. Massaro, R. Bretherton, W. Stoppel, D. L. Kaplan, A. Balduini, *Biomaterials* **2018**, *178*, 122.
[22] N. Somsesta, V. Sricharoenchaikul, D. Aht-Ong, *Mater. Chem. Phys.* **2020**, *240*, 122221.
[23] T. Lu, X. Xu, S. Zhang, L. Pan, Y. Wang, S. M. Alshehri, T. Ahamad, M. Kim, J. Na, M. S. A. Hossain, *Bull. Chem. Soc. Jpn.* **2020**, *93*, 1014.

[24] Y. Guo, H. Lu, F. Zhao, X. Zhou, W. Shi, G. Yu, *Adv. Mater.* **2020**, *32*, 1907061.
[25] T. D. Quilichini, E. Grienenberger, C. J. Douglas, *Phytochemistry* **2015**, *113*, 170.
[26] P. Gonzalez-Cruz, M. J. Uddin, S. U. Atwe, N. Abidi, H. S. Gill, *ACS Biomater. Sci. Eng.* **2018**, *4*, 2319.
[27] S. Bernard, K. Benzerara, O. Beyssac, E. Balan, G. E. BrownJr., *Heliyon* **2015**, *1*, e00034.
[28] M. Bagcioglu, B. Zimmermann, A. Kohler, *PLoS One* **2015**, *10*, e0137899.
[29] E. Katifori, S. Alben, E. Cerda, D. R. Nelson, J. Dumais, *Proc. Natl. Acad. Sci. USA* **2010**, *107*, 7635.
[30] T. Liu, Z. Zhang, *Biotechnol. Bioeng.* **2004**, *85*, 770.
[31] F. S. Li, P. Phyo, J. Jacobowitz, M. Hong, J. K. Weng, *Nat. Plants* **2019**, *5*, 41.
[32] H. Wang, M. G. Potroz, J. A. Jackman, B. Khezri, T. Marić, N.-J. Cho, M. Pumera, *Adv. Funct. Mater.* **2017**, *27*, 1702338.
[33] R. C. Mundargi, M. G. Potroz, S. Park, H. Shirahama, J. H. Lee, J. Seo, N. J. Cho, *Small* **2016**, *12*, 1167.
[34] K. Fang, Y. Wang, T. Yu, L. Zhang, F. Baluška, J. Šamaj, J. Lin, *Flora* **2008**, *203*, 332.
[35] T. F. Fan, S. Park, Q. Shi, X. Zhang, Q. Liu, Y. Song, H. Chin, M. S. B. Ibrahim, N. Mokrzecka, Y. Yang, H. Li, J. Song, S. Suresh, N. J. Cho, *Nat. Commun.* **2020**, *11*, 1449.
[36] Z. Zhao, Y. Hwang, Y. Yang, T. Fan, J. Song, S. Suresh, N. J. Cho, *Proc. Natl. Acad. Sci. USA* **2020**, *117*, 8711.
[37] C. S. Pomelli, F. D'Andrea, A. Mezzetta, L. Guazzelli, *New J. Chem.* **2020**, *44*, 647.
[38] X. Xie, Y. Zhou, H. Bi, K. Yin, S. Wan, L. Sun, *Sci. Rep.* **2013**, *3*, 2117.
[39] W. Chen, Y.-X. Huang, D.-B. Li, H.-Q. Yu, L. Yan, *RSC Adv.* **2014**, *4*, 21619.
[40] Z. Wu, Y. Li, L. Zhang, Y. Zhong, H. Xu, Z. Mao, B. Wang, X. Sui, *RSC Adv.* **2017**, *7*, 20147.
[41] L. Guo, Z. Chen, S. Lyu, F. Fu, S. Wang, *Carbohydr. Polym.* **2018**, *179*, 333.
[42] Y. Zhang, S. Wang, M. Eghtedari, M. Motamedi, N. A. Kotov, *Adv. Funct. Mater.* **2005**, *15*, 725.
[43] P. I. Dolez, M. A. Arfaoui, M. Dubé, É. David, *Proc. Eng.* **2017**, *200*, 81.
[44] Z. Hu, X. Zen, J. Gong, Y. Deng, *Colloids Surf., A* **2009**, *351*, 65.
[45] Y. Chen, X. Zhang, B. Wang, M. Lv, Y. Zhu, J. Gao, *RSC Adv.* **2017**, *7*, 15625.
[46] S. J. Charde, S. S. Sonawane, S. H. Sonawane, S. Navin, *Chem. Eng. Commun.* **2018**, *205*, 492.
[47] S. R. B. L. Yule, J. E. A. Marshall, *Org. Geochem.* **2000**, *31*, 859.
[48] R. Fu, B. Zheng, J. Liu, M. S. Dresselhaus, G. Dresselhaus, J. H. Satcher, T. F. Baumann, *Adv. Funct. Mater.* **2003**, *13*, 558.
[49] O. Laitinen, T. Suopajarvi, M. Osterberg, H. Liimatainen, *ACS Appl. Mater. Interfaces* **2017**, *9*, 25029.
[50] E. L. Tan, M. G. Potroz, G. Ferracci, J. A. Jackman, H. Jung, L. Wang, N. J. Cho, *Adv. Funct. Mater.* **2018**, *28*, 1707568.